# Effects of fast charging on hybrid lead/acid battery temperature

T.G. Chang, E.M. Valeriote and D.M. Jochim
*Cominco Ltd., Product Technology Centre, Mississauga, Ont., L5K 1B4 (Canada)*

**Abstract**

The effects of very fast charging on two types of deep-cycling hybrid lead/acid batteries were determined using a MINITCHARGER™ to control the charging current. One of the hybrid batteries was flooded and contained Pb–4.7wt.%Sb positive grids, the other was a valve-regulated battery with Pb–1.5wt.%Sb–0.3wt.%Sn positive grids. Results are presented and discussed in relation to these battery types, but many of the conclusions are more generally applicable. It was found that both 5-min/50%-recharge and 15-min/80%-recharge rates could be achieved, in the case of the flooded battery, with a quite acceptable temperature increase. Following an 80% depth-of-discharge, the dominant source of heat was ohmic during the first 40% of the charge returned at very high rates. The temperatures were distributed non-uniformly within the battery. After this, non-ohmic polarization became progressively more important. For the hybrid recombination battery, the oxygen cycle is a substantial source of heat during the latter stages of the charge, particularly in comparison with previous non-antimonial batteries that have been investigated.

## Introduction

It is generally agreed that if electric vehicles were to replace vehicles powered by internal combustion engines, atmospheric pollution could be greatly alleviated, especially around population centres. California has passed a law that requires, in 1998, 2% of all new vehicles sold in the state to be zero-emission vehicles. The percentage will be increased to 10% by 2003 and other US states have or are expected to follow California. Accordingly, current interest in electric vehicles is quite intense. At present, the most likely candidate battery to power these vehicles, and be produced in the required commercial quantities, is the lead/acid system. Because of its relatively low energy density, a vehicle powered by lead/acid batteries can only travel about 100 to 200 km between charges. This limited range of travel would not readily be accepted by consumers in North America. If the battery packs in the vehicles could be rapidly recharged, however, the daily total range of travel could be greatly extended without unacceptable idle times at charging stations.

Methods for the rapid charging of lead/acid batteries have long been sought. In 1973, Gross [1] published a review that outlined earlier work on theoretical considerations, and discussed requirements and methods of rapid charging. One of the rapid-charging techniques, namely, constant resistance-free voltage charging, had been discussed in detail by Kordesch [2]. A fast charger based on this principle was recently patented by Norvik Inc. [3]. Studies of rapid charging using this particular charging method have been carried out with the Norvik MINITCHARGER™ at Cominco's Product Technology Centre and elsewhere [4–7]. Results from our investigation of non-antimonial

0378-7753/94/$07.00 
*SSDI* 0378-7753(93)01864-E

lead/acid batteries have already been reported [8]. In this paper, a study of fast-charging effects on hybrid lead/acid batteries, that contained antimonial positive grids and non-antimonial negative grids, is discussed.

## Experimental

*Batteries*

Two types of hybrid batteries were tested. Batteries of the first type, which will be referred to as "AP" in this report, were flooded 12-V batteries. The positive grids were gravity cast and made from Pb–4.7wt.%Sb alloy. The negatives were expanded and made from Pb–0.1wt.%Ca–0.3wt.%Sn alloy. Each cell contained five positive and six negative plates. The positive plates were each wrapped in a glass mat and a microporous polyethylene (DARAMIC®) separator. There was much more positive (~800 g) than negative (~540 g) active material in each cell. The battery was designed for deep-discharge applications and had a capacity of 80 Ah at the 20-h rate.

The other batteries tested were of the valve-regulated type, using absorptive glass-mat separators. They will be referred as "ST" batteries. Each cell contained five positive and six negative plates. The positive plates had gravity-cast Pb–1.5wt.%Sb–0.3wt.%Sn grids. The negative grids were cast from Pb–0.12wt.%Ca–0.4wt.%Sn alloy. These batteries were also recommended by the manufacturer for deep-cycling applications.

The internal resistances of the test batteries and their discharge capacities are listed in Table 1.

*Equipment and software*

A MINITCHARGER™ (Model MC36-300A, Norvik Technologies Inc., Mississauga, Ont., Canada) was used in this investigation. It maintained the resistance-free voltage during charging at the constant level set by the operator, biased to compensate for temperature deviations from 25 °C. The discharge of the test batteries was controlled by a 1250 W electronic load (Lectra-Load II, Model LL300B, RTE Power/Mate, Hackensack, NJ). The test was monitored and controlled by a personal computer (PC). Analog inputs/outputs and digital outputs were conducted through a DAS-16G card (Keithley Metrabyte Corporation, Taunton, MA) installed in the computer. Temperature sensors were type-K thermocouples connected to Fluke 80TK thermocouple modules (John Fluke Mfg. Co. Inc., Everett, WA). The pressure sensor was a thin-film polysilicon current-loop transducer (Model PX605, Omega Engineering, Stamford, CT).

*Test conditions*

Test batteries were discharged at the $C_3/3$ rate (where $C_3$ is the capacity at the 3-h discharge rate) and were charged at a constant resistance-free voltage ($V_{ref}$) for 1 h, and then at a higher voltage for 3 to 4 h to complete the charging. Thermocouples were inserted into the battery to measure the internal temperatures. The external temperatures were taken from a thermocouple placed between a piece of insulating sponge and the surface of a side-wall. No artificial means of cooling was applied to the batteries during testing.

## Results and discussion

To avoid any confusion, rapid (fast) charging is defined in this study as a charge process that will return 50, 80 and 100% of the previous discharge within 5, 15, and

TABLE 1

Internal resistance and discharge capacity of test batteries

| Battery code | Type | Internal resistance (mΩ) | | | Discharge capacity | | | | | | Weight (kg) |
|---|---|---|---|---|---|---|---|---|---|---|---|
| | | Fully charged | 80% discharge | 100% discharge | 1-h rate ($C_1$/1) | | 3-h rate ($C_3$/3) | | 5-h rate ($C_5$/5) | | |
| | | | | | (A) | (Ah) | (A) | (Ah) | (A) | (Ah) | |
| ST | 12-V, absorptive glass-mat, valve-regulated grid: (+) 1.5wt.%Sb–0.3wt.%Sn (−) 0.12wt.%Ca–0.4wt.%Sn | 3.3 | 4.7 | 6.9 | 39.3 | 39.3 | 17.5 | 52.5 | 10.9 | 54.5 | 22.35 |
| AP | 12-V, flooded (+) 4.7wt.%Sb (−) 0.1wt.%Ca–0.3wt.%Sn | 5.4 | 7.2 | 9.3 | 38.1 | 38.1 | 17.0 | 50.9 | 11.7 | 54.4 | 20.30 |

TABLE 2

Conditions of fast charging (return of 50% of previous discharge within 5 min, and 80% within 15 min) for test batteries with 80% depth-of-discharge. Also shown are cases where 80%, but not 50%, criterion is met

| Battery | Maximum current (A) | Charge rate (C) | Return 80% within 15 min only | | | | Return of 50% within 5 min and 80% within 15 min | | | | |
|---|---|---|---|---|---|---|---|---|---|---|---|
| | | | $V_{ref}$ (V) | Actual return (%) | Peak temperature (°C) | Temperature rise (°C) | $V_{ref}$ (V) | 5 min actual return (%) | 15 min actual return (%) | Peak temperature (°C) | Temperature rise (°C) |
| AP63 | 200 | 4.0 | 14.85 | 82.7 | 47.6 | 17.3 | | | | | |
| | 250 | 5.0 | | | | | 14.70 | 50.2 | 81.1 | 57.6 | 25.8 |
| AP64 | 150 | 2.9 | 14.70 | 78.6 | 45.7 | 15.7 | | | | | |
| | 300 | 5.9 | | | | | 14.70 | 55.0 | 82.7 | 55.8 | 26.0 |
| ST2 | 150 | 2.9 | 15.00 | 82.0 | 61.1 | 31.0 | | | | | |
| | 200 | 3.8 | 14.85 | 78.2 | 57.7 | 28.1 | | | | | |
| | 250 | 4.8 | | | | | 14.40 | 48.2 | 81.1 | 56.8 | 24.7 |
| | 300 | 5.7 | | | | | 14.70 | 57.0 | 92.7 | 64.6 | 35.2 |

240 min, respectively. This is similar, but not identical, to the fast-recharge goals of the Advanced Lead-Acid Battery Consortium. These goals appear to be based on a 100% depth-of-discharge (DOD) [9]. For the work reported here, an 80% DOD was used in most cases.

*Flooded hybrid battery AP*

It was found that these flooded batteries could be rapidly recharged with quite acceptable temperature increases. As shown in Table 2, if only the 15-min/80%-return was required, the internal battery temperature remained well below 50 °C when the charge was commenced at 30 °C. If both the 5-min/50%-return and the 15-min/80%-return requirements had to be satisfied, the temperature rise during the charge was 26 °C.

Figure 1 shows typical profiles of a rapid-charge cycle for an AP battery (AP63). This cycle comprised charging, followed by a rest, discharging, and another rest before being charged again. The current limit was 250 A, the $4.9C_3$ rate. The battery was being rapidly recharged: 50% of the previous discharge was returned in 5 min and 80% in 15 min. The internal temperature peaked quickly at 57 °C in 5 min. The external temperature lagged behind, and reached a maximum of 47 °C after 37 min of charging. After 1 h of charging, the reference voltage was raised from 14.7 to 15.9 V to complete the charging. After 4 h of charging, the battery was left resting for 10 min before being discharged at 16.6 A (i.e., at the $C_3/3$ rate) for 2.4 h to reach an 80% DOD. Five minutes after the completion of the discharge, the battery was charged again.

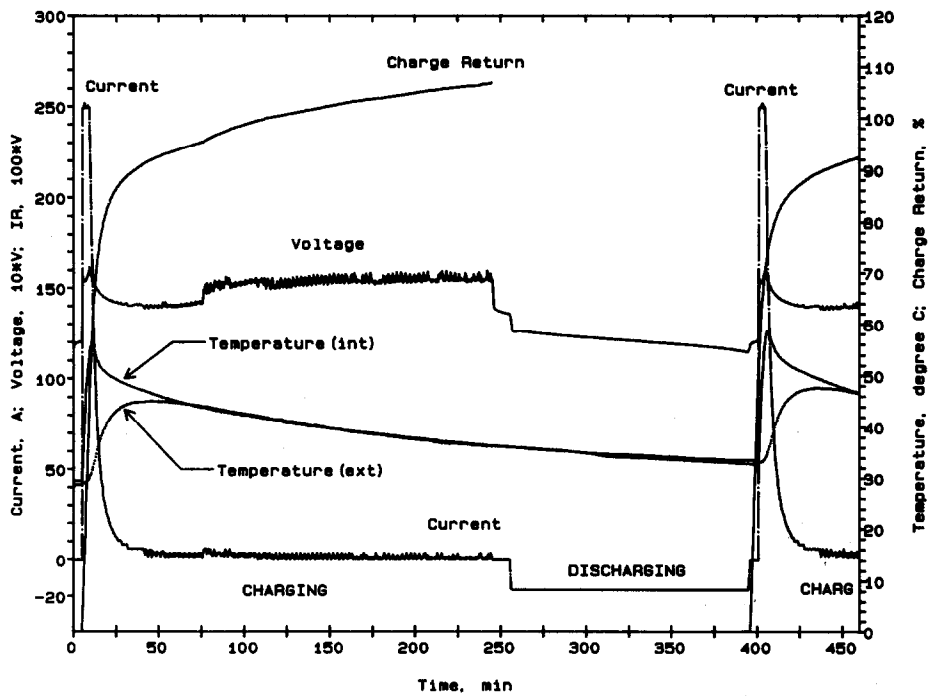


Fig. 1. Battery AP63 in rapid-charge cycling (cycle 52). Charging: current limit = 250 A; charging $V_{ref}$ = 2.45 V/cell for 1 h; 2.65 V/cell for 3 h. Discharging: 16.5 A to 80% DOD.

More detailed profiles of charging voltage, current, temperatures and charge return for battery AP64 are given in Fig. 2. The constant resistance-free charging voltage was set at 14.7 V. After the charging was started, the charging voltage was raised quickly and automatically by the charger to a little over 16 V; this included compensation for the ohmic voltage-drop. As the charging proceeded, the internal resistance of the battery decreased, so that the charging voltage to maintain the 300-A charging current was correspondingly reduced by the charger. As more charge was returned, however, the polarization increased; therefore, the charger had to increase the applied voltage in order to maintain the 300-A current. After 3.5 min of charging, the resistance-free voltage limit was reached at an applied charging voltage of 16.5 V. After that, the polarization continued to grow and this made the 300-A current level unsustainable at this voltage limit. As a consequence, the current quickly declined, not only because the polarization was increasing, but because the charging voltage was also being reduced as the ohmic voltage-drop decreased with decreasing current. Within 30 min, the current had declined to a very low level and the charging voltage became essentially the same as the reference voltage, including temperature compensation.

There are three internal-temperature profiles shown in Fig. 2. They were taken from different locations, all within a central cell of the battery. t_int1 was situated right at the centre, both length-wise and thickness-wise, of the plate assembly, and about 2.5 cm from the top of the plates. t_int2 was also in the centre of the plate-stack thickness-wise, about 1 cm from the top of the plates, but close to the side of the battery, about 4 cm from the vertical edge of the plates. The third thermocouple,

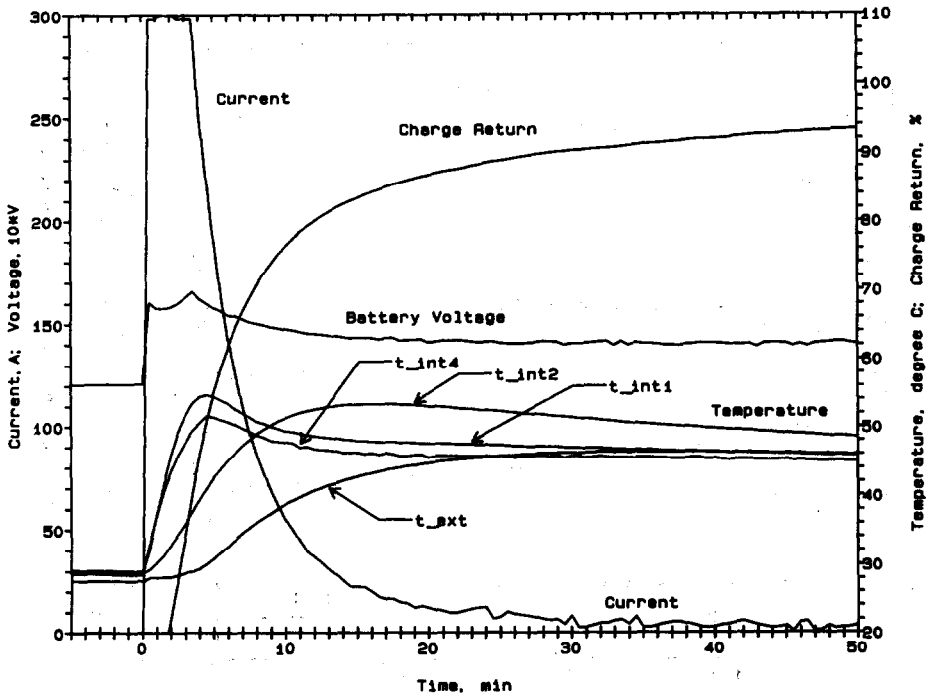


Fig. 2. Temperatures, voltage, current and charge return for battery AP64. Charging: $V_{ref}$ = 2.45 V/cell; $I$ = 300 A max; temperature compensation = 6 mV/°C per cell; DOD of previous discharge = 80%.

t_int4, was placed between the plate assembly and the inter-cell partition, about 5 to 6 cm from the top. The temperature profiles show that the temperature at the centre of the plate assembly, at least in the top part of it, where the thermocouples t_int1 and t_int2 were located, shot up rapidly, at a rate of 10 °C/min. Within 4.5 min, the temperature at the centre of the plate assembly peaked at 56 °C; then it dropped below 50 °C in about 5 min. In contrast, the temperature between the plate assembly and the inter-cell partition rose at a much lower rate, namely, 3 to 4 °C/min, and peaked at 54 °C after about 15 min of charging. The temperature on the side-wall of the battery, t_ext, lagged behind all the internal temperatures. It rose gradually to a maximum of 46 °C after about 40 min of charging.

Some complexity of the internal temperature profiles is shown in Fig. 3. The data represent three temperature profiles for charging with current limits of 150, 200 and 300 A, respectively. All temperatures rose at a high rate from an initial temperature of about 30 °C, then slowed down, and then rose faster again. Inflexion points all occurred when about 40% of the previous discharge had been returned. This phenomenon was also observed in antimony-free batteries [8] and it was concluded that there must be some heat sources other than ohmic that provided the heat for the re-acceleration of the temperature increase.

The temperature increase of a battery depends, of course, on the rate at which heat is generated within it. If the heat dissipation to the environment is ignored, the rate of temperature increase can be expressed as:

$$dT/dt = 1/C_p(dq/dt) \quad (1)$$

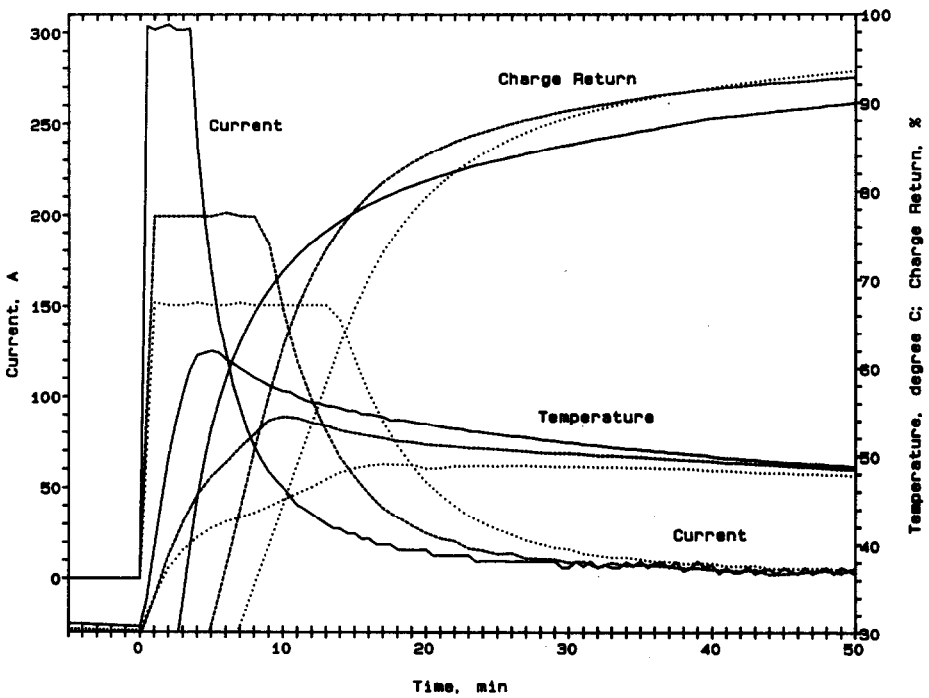


Fig. 3. Currents, charge and internal temperatures for battery AP63, charged at currents of: (·····) 150 A; (----) 200 A; (——) 300 A.

where $T$ is the temperature, $t$ the time, $C_p$ the heat capacity of the battery, and $q$ the heat.

Equation (1), can also be expressed as [10, 11]:

$$dT/dt = 1/C_p[I(V-V_o) - I(T/nF)(\partial S/\partial \xi)] \quad (2)$$

where $I$ is the current, $V$ the cell voltage, $V_o$ the open-circuit voltage, $n$ the number of electrons involved in the reaction, $F$ the Faraday constant, $S$ the entropy, and $\xi$ reaction progress variable (molar fraction).

The last term on the right-hand-side of eqn. (2) involves entropy and is the reaction heat, which is only about 3% of the free energy change for the process. It has been shown [4] previously that this reaction heat is very small compared with resistive heat.

The first term in eqn. (2), $I(V-V_o)$, is the total Joule effect and can be partitioned into:

$$I(V-V_o) = I^2R + I\eta \quad (3)$$

where $\eta$ is the non-ohmic polarization overpotential, and $R$ the resistance of the cell. Thus, combining eqns. (2) and (3) gives:

$$dT/dt = 1/C_p[I^2R + I\eta - I(T/nF)(\partial S/\partial \xi)] \quad (4)$$

The heat that causes the temperature rise comes mainly from two sources (the ohmic heat and the heat caused by non-ohmic polarization) since the reaction heat is very small in comparison.

When the initial rate of temperature increase in the battery (before 40% return) is plotted against the square of the charging current, as shown in Fig. 4, an approximately linear relation is revealed. This finding suggests that, in the initial period of charging ohmic heating is dominant.

During charging, the ohmic voltage drop, IR, was continuously measured by taking advantage of the current-interruption routine in the MINITCHARGER's charging process. From the ohmic-drop data, the values of the ohmic heating rate, $I^2R$, were calculated. This analysis for battery AP64, which was charged at a constant resistance-free voltage of 15.0 V with a current limit of 300 A (the $6C_3$ rate), is illustrated in Fig. 5. It can be seen that, at 300 A, the total Joule effect of 900 W was substantial, and 71% of it was manifested as ohmic heating. In the first 2 min, the ohmic heating rate decreased continuously, then it stayed constant until the current started to fall. In contrast, the total Joule effect only declined a little in the first moments, and then increased sharply after that. The difference between the two is the non-ohmic heating, $I(V-V_o) - I^2R$. This factor was only 29% at the beginning, and grew to 50% when the current started to decrease. From then on, although both ohmic and non-ohmic heating decreased, ohmic heat production declined at a higher rate. Therefore, the non-ohmic heating soon became dominating. After 70% of the previous discharge had been returned, the contribution from the ohmic source became minor. The analysis clearly shows that acceleration of the temperature increase, as shown in Fig. 3, at about the time when 40% of the previous discharge had been returned, could be ascribed to the non-ohmic polarization. If a lower current limit had been used, the relative contribution from polarization heat would have been larger. For instance, with the current limit set at 150 A ($3C_3$ rate), when 40% of the previous discharge had been returned, the contribution from non-ohmic polarization was twice as large as that from the ohmic loss.

In the above analysis, it was assumed that there were no side-reactions. Observations made in this study clearly indicated that this was not the case. When charging at high

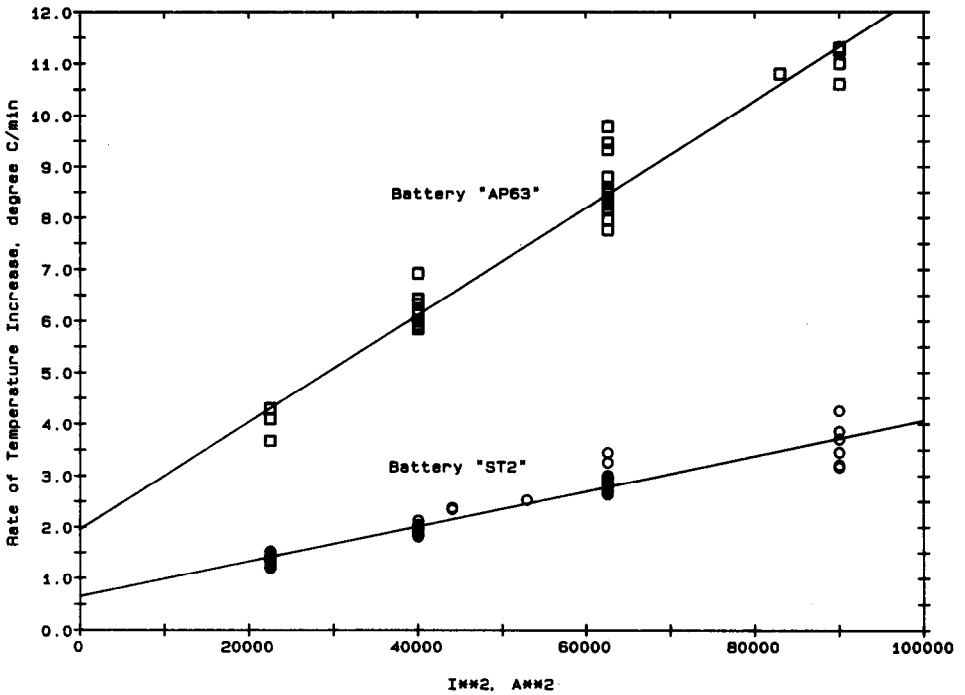


Fig. 4. Dependence of initial rate of temperature increase on square of charging current.

current limits, some gassing was always observed from the very beginning. When about 40% of the previous discharge had been returned, gassing in the flooded batteries was quite vigorous. The decomposition of water is thermodynamically endothermic. Due to the high overvoltage for the battery reaction, however, about 40 to 50% of the net energy used for water electrolysis is dissipated as heat.

One of the AP batteries was cycle-tested to failure. It achieved 74 cycles before the discharge capacity had declined to 80% of the initial value. Up to then, no antimony poisoning apparently occurred, since the end-of-charge current was always low. When the battery failed, the discharge capacity was negative-plate limited in every cell. It was observed that most of the negative active material had contracted to leave gaps around the pellets.

*Recombination hybrid battery ST*

Batteries of the hybrid (ST) type accepted rapid recharge quite well. The resulting temperatures were higher, however, than those for the batteries AP discussed above. It was difficult to keep the temperature under 50 °C when the ST batteries were charged to meet the 5-min/50%-return and 15-min/80%-return requirements.

A charging profile for battery ST2, which was charged at a constant resistance-free voltage of 2.40 V/cell (14.4 V/battery) with a current limit of 250 A, is depicted in Fig. 6. All the curves are very similar to those for battery type AP. Since ST batteries are recombination valve-regulated types, the internal pressure was also monitored. Figure 6 shows that the pressure in the battery increased slowly during the first 3 min of charging. At about the time when 40% of the previous discharge had been returned, the pressure increase accelerated quite abruptly; this indicated

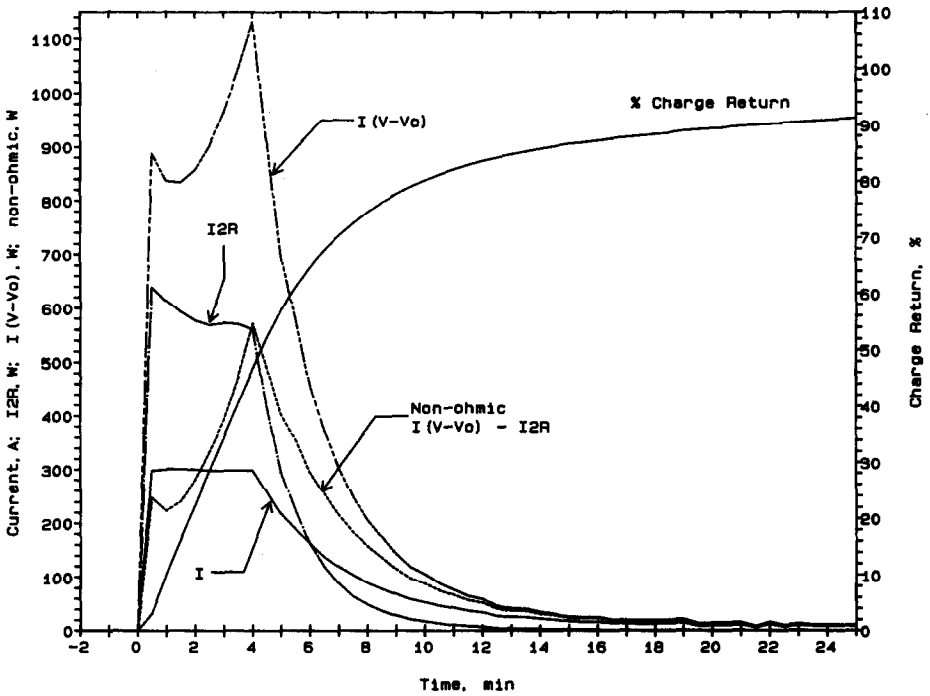


Fig. 5. Analysis of heat generated by Joule effect in battery AP64 (cycle 43). Charging: $V_{ref}$ = 2.50 V/cell; $I$ = 300 A max; DOD of previous discharge = 80%.

the commencement of water decomposition. At the sixth minute of charging, the release pressure of the valves was reached. Thereafter, pressure decreased slowly with the decreasing current. Recombination reactions must have been faster than gas evolution during this period.

For comparison, the charging of batteries AP64 and ST2 are both given in Fig. 7. Both were charged at a constant resistance-free voltage of 2.45 V/cell (14.7 V/battery) with a current limit of 300 A. Both met the requirements for rapid charging. In the initial 3 min, the charging voltage for AP64 was about 1 V higher than that for ST2. This is equivalent to a difference in internal resistance of about 3 mΩ for these two batteries, a value that is only slightly higher than the measured resistance differences given in Table 1. This was reflected in greater ohmic heating and a much higher rate of temperature increase for AP64. The current for AP64 started to decline from the 300-A level after 3 min of charging, and the temperature began to decrease after 4 min. In comparison, the current for ST2 started to decline only after 4 min of charging, and it was higher than that for AP64 throughout the rest of the charging period. It is noteworthy that, at the time when the current for ST2 decreased, the rate of the temperature increase became greater. After 6 min, although the temperature was still rising, the rate of increase began to decline. The temperature started a slow decline only after about 20 min of charging. The comparison of the temperature patterns of AP64 and ST2 strongly suggests that the difference between them could be ascribed to the heat generated from the oxygen cycle in ST2. The cycle started at about 40% return, as indicated by an abrupt increase in gas pressure in the battery. The energy spent on the oxygen cycle is completely (100%) converted into heat, in

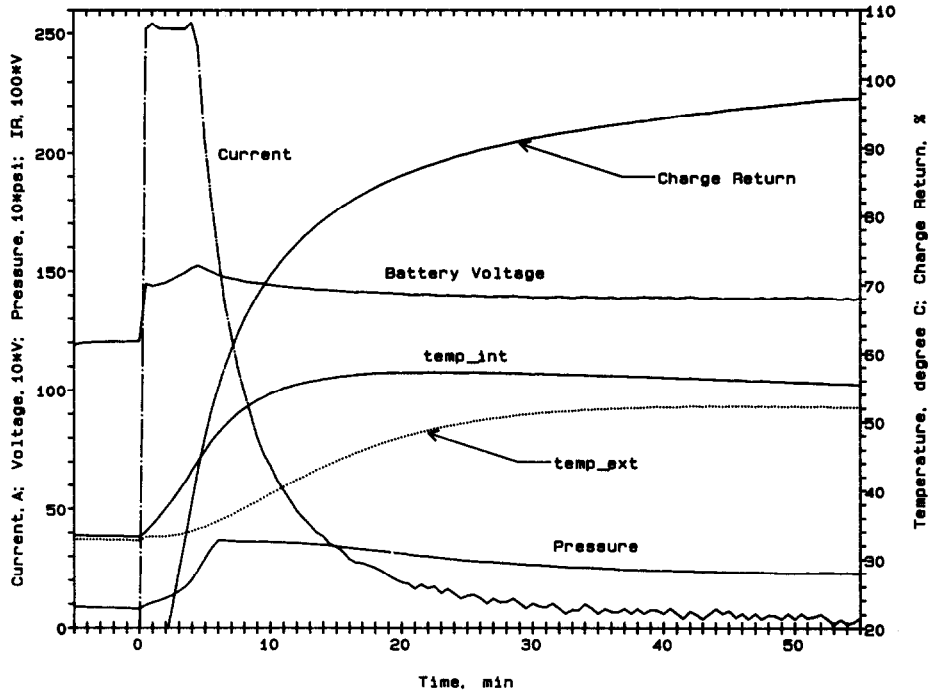


Fig. 6. Temperatures, voltage, current, pressure and charge return of battery ST2 in rapid charging (cycle 59). Charging $V_{ref}=2.40$ V/cell; $I=250$ A max; temperature compensation = 4 mV/°C; DOD = 80%.

comparison with about 40% for water decomposition alone. Furthermore, because of oxygen reduction, the negative plates are depolarized. Thus, with the same constant resistance-free voltage, ST2 accepted a higher current, which generated even more heat.

In spite of all the differences, the plot of the initial rate of temperature increase in battery ST2 against the square of charging current, as shown in Fig. 4, suggests a linear relationship. (It should be noted that the rates of temperature increase for the two batteries plotted in Fig. 4 are not strictly comparable, because the temperature probes used to generate the data were not at the same location.) This again suggests that, in the initial period, ohmic heat was the dominant heat source.

In addition to greater heat generation, another disadvantage for the ST batteries compared with AP batteries, in limiting temperature increase, arises because the latter were flooded, and so contained much more electrolyte. Equation (1) shows that, for a given amount of heat, the battery that has a larger heat capacity will have a smaller temperature rise. Sulfuric acid solutions have a heat capacity which is much more than 10 times that of lead, lead dioxide or lead sulfate. In addition, compared with the partly-filled glass mat, the free sulfuric acid solution in the AP batteries should be much better in transferring heat from hotter to cooler locations. This includes transfer to the battery case where the heat can be dissipated to the environment.

One of the ST batteries was cycle-tested to failure. It lasted 99 cycles, when its capacity decreased to 80% of the original value. No obvious cause for capacity decline

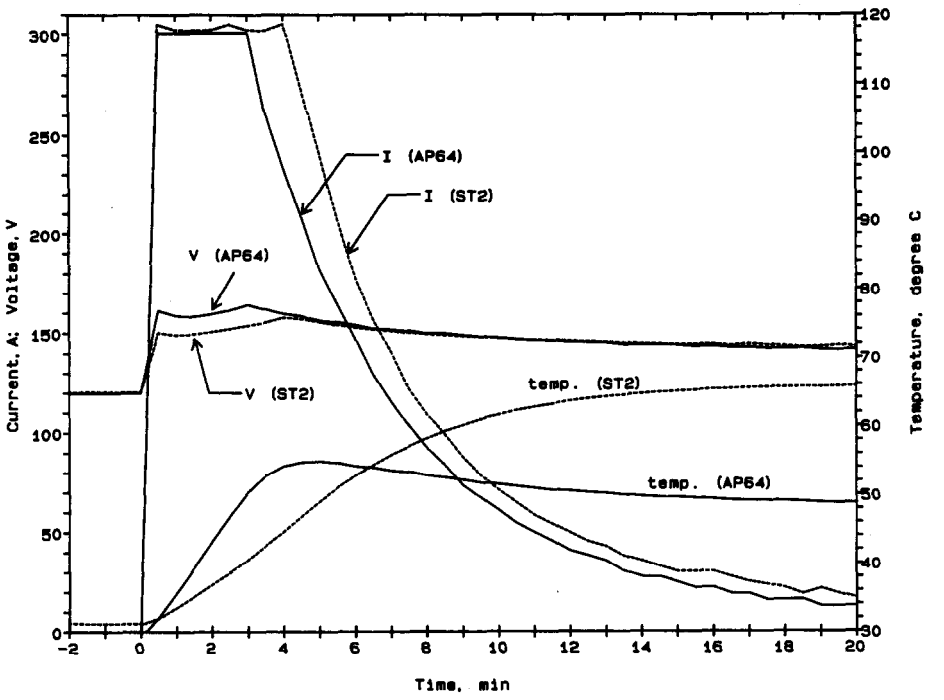


Fig. 7. Comparison of batteries AP64 and ST2. Charging: $V_{ref}$=2.45 V/cell; $I$=300A max; DOD=80%.

was found. It is suspected, however, that loss of electrolyte might have been the cause of failure.

## Conclusions

1. The temperature distribution in batteries subjected to rapid charging appeared to be non-uniform, with possible development of temporary localized hot spots.

2. In the first part of a rapid charge to about 40% return, at a current larger than $2.6C_3$, the dominant heat source is ohmic. Therefore, if a battery is designed to meet the 5-min/50%-return requirement, the best strategy is to design a battery of low internal resistance.

3. After the 40% return point, the heat from non-ohmic sources becomes progressively more important.

4. If the rapid charge has to return more than 40% of the previous discharge, the oxygen cycle might generate an undesirable amount of heat in batteries of the recombination type, especially if they are not antimony-free.

5. A battery that has a larger heat capacity will have a lower temperature rise when subjected to rapid charging, if all other conditions are the same. Therefore, batteries of the flooded type will have a lower temperature rise, since sulfuric acid solutions have a large heat capacity. Flooded batteries will also have less heat production from water decomposition, and better heat transfer to the battery exterior.

**Acknowledgements**

Supply of the MINITCHARGER™ and technical assistance by Norvik Technologies Inc. and the financial support of the Advanced Lead-Acid Battery Consortium are gratefully acknowledged.

**References**

1 S. Gross, *Proc. Conf. 8th Annual Meet. of IEEE Industry Applications Society, Milwaukee, WI USA, Oct. 8–16, 1973,* Institute of Electric and Electronic Engineers, Piscataway, NJ, USA, 1973, pp. 905–912.
2 K. Kordesch, *J. Electrochem. Soc., 113* (1972) 1053.
3 J.K. Nor, *EP Patent No. 0 311 460 A2* (Oct. 10, 1988); *US Patent No. 5 202 617* (Apr. 13, 1993).
4 E.M. Valeriote, J.K. Nor and V.A. Ettel, *Proc. 5th Int. Lead/Acid Battery Seminar,* International Lead Zinc Research Organization (ILZRO), Inc., Research Triangle Park, NC, USA, 1991, pp. 93–122.
5 E.M. Valeriote and D.M. Jochim, *J. Power Sources, 40* (1992) 93.
6 J.K. Nor, *Proc. 25th Int. Symp. Automotive Technology, Florence, Italy, June 1–5, 1991.*
7 J.K. Nor, *Proc. 11th Int. Electric Vehicle Symp., Florence, Italy, Sept. 27–30,* 1992, Sym. Proc. Vol. 1, paper No. 9.03.
8 T.G. Chang, E.M. Valeriote and D.M. Jochim, *Proc. 26th Int. Symp. Automotive Technology, Aachen, Germany, Sept. 13–17, 1993,* pp. 405–413.
9 J.F. Cole, *J. Power Sources, 40* (1992) 1.
10 H.F. Gibbard, *J. Electrochem. Soc., 125* (1978) 353.
11 D. Berndt and E. Meissner, *Proc. 12th Int. Telecommunication Energy Conf., Orlando, FL, USA, 1990,* Institute of Electric and Electronic Engineers, Piscataway, NJ, USA, 1990, pp. 1–7.